Data-Aided Carrier Phase Estimation for GMSK

Michael Rice
Department of Electrical & Computer Engineering
Brigham Young University
Provo, UT
mdr@ee.byu.edu

Bill McIntire and Osama Haddadin
L-3 Communications, Communication Systems – West
Salt Lake City, Utah
william.k.mcintire@l-3com.com
osama.s.haddadin@l-3com.com

***Abstract*— This paper examines the bias in data-aided maximum-likelihood carrier phase estimation for GMSK based on a linear detector structure using only the first Laurent pulse. The bias in the ML phase estimate increases with decreasing BT_b and decreasing training sequence length. Three methods for bias compensation are described and their performance examined. Simulation results show that the performance of the bias compensation techniques can achieve the Cramer-Rao bound.**

I. INTRODUCTION

Gaussian Minimum Shift Keying (GMSK) is a popular modulation for bandwidth-constrained systems using non-linear amplifiers. Since GMSK is a constant envelope modulation, non-linear amplification does not produce spectral "regrowth" in the transmitted waveform. The continuous phase transitions, smoothed by a Gaussian low-pass filter, produce a modulated signal with good spectral properties. The 3-dB bandwidth of the Gaussian filter can be adjusted to provide the system designer with a trade-off between detection efficiency (i.e. power) and occupied bandwidth.

Let $z(t)$ be the complex envelope of the GMSK modulation waveform given by

$$z(t) = \exp\{j\phi(t;\boldsymbol{\alpha})\} \tag{1}$$

where

$$\begin{aligned} \phi(t;\boldsymbol{\alpha}) &= \pi h \sum_n \alpha_n g(t - nT_b) \\ \alpha_n &\in \{-1,+1\} \\ g(t) &= \int_{-\infty}^{t} f(x)dx \end{aligned} \tag{2}$$

where $f(x)$ is the frequency pulse shape which is a function of a unit-area Gaussian pulse with 3-dB bandwidth B and which is truncated to a length LT_b. In practice LT_b is usually set to $1/B$ [1]. For minimum shift keying, the modulation index $h = 1/2$.

An alternate amplitude modulated pulse (AMP) representation due to Laurent [2] is also possible. In this representation, $z(t)$ is expressed as the superposition of 2^{L-1} time and phase shifted amplitude modulated pulses:

$$z(t) = \sum_{k=0}^{2^{L-1}-1} \sum_n a_{k,n} h_k(t - nT_b). \tag{3}$$

In the Laurent decomposition, the $a_{k,n}$ are the pseudo-symbols which are related to the channel symbols α_n and the modulation index h as given in [2]. The $h_k(t)$ are the amplitude pulses which are a function of $g(t)$, h, and L as explained in [2].

The Laurent AMP representation suggests a linear detector structure consisting of 2^{L-1} matched filters: one filter matched to each of the Laurent pulses $h_k(t)$. Since the pulses $h_k(t)$ do not satisfy the Nyquist no-ISI condition [3], maximum likelihood sequence estimation using the 2^{L-1} parallel matched filter outputs is required [4].

The Laurent representation also provides a guide for studying the performance versus complexity trade-off. The detector structure can be simplified by truncating the Laurent representation to fewer than 2^{L-1} pulses. Kaleh [4] demonstrated that a linear detector for GMSK with $BT_b = 1/4$ and $L = 4$ based on 2 matched filters rather than $2^{L-1} = 8$ matched filters achieves the performance of the optimal detector for all practical purposes. This result was confirmed by Tsai and Lui [1] who also showed that using a linear detector based on filters matched to the first two Laurent pulses provides nearly optimal performance for $BT_b \geq 1/5$.

Simple linear detectors based on the first Laurent pulse have also been examined in [4-8] under the names "serial detector" [5-6], "threshold detector" [7], and "MSK-type detector" [8]. In general, the performance of this approach is worse than that of the detector using two matched filters, especially as BT_b gets smaller. In these cases, the ISI increases so that a Viterbi-based ML sequence estimator [4-6] or equalizer [5] must follow the matched filter. One intriguing exception to this trend is the case of severe adjacent channel interference. In this case, the serial detector with an equalizer outperforms the detector based on the first 2 Laurent pulses. This is due to the inclusion of the second Laurent pulse in the detector. It has a wider bandwidth than the first pulse thus allowing more energy from the adjacent channels into the decision making process [5].

Carrier phase synchronization for GMSK has been studied both in theory [6,8-10] and in practice [11]. Data-aided techniques were addressed in [6,8,10]. In [8], the data-aided ML carrier phase estimator is derived assuming a serial or MSK-type detector. The phase lock-loop-based phase estimator in [6] bases the phase error signal on the same quantity. In [10], an alternate representation of CPM in terms of time-limited sinusoidal basis functions is examined.

0-7803-7802-4/03/$17.00 © 2003 IEEE

Given the attractive features of the serial detector using a single filter matched to the first Laurent pulse, this paper focuses on data-aided carrier phase estimation assuming that structure. We extend the results in [8] by showing that the "edge effects" result in a biased estimate. Once this bias is removed, the performance of the ML estimator is able to achieve the Cramer-Rao bound.

II. Serial Detector Structure

The serial detector, shown in Figure 1 consists of a filter matched to the first Laurent pulse $h_0(t)$ given by

$$h_o(t) = \prod_{i=0}^{L-1} c(t - iT_b - LT_b) \tag{4}$$

where, for $h = 1/2$, $c(t)$ is given by

$$c(t) = \begin{cases} \cos\left(\frac{\pi}{2} g(|t|)\right) & |t| \le LT_b \\ 0 & |t| > LT_b \end{cases}. \tag{5}$$

The filter $h_0(t)$ spans $(L+1)T_b$ seconds and introduces ISI spanning $L+1$ symbols. The matched filter output $x(t)$ is sampled at the bit rate, or every T_b seconds. For large values of BT_b, the sign of $x(kT_b)$ can be used as the decision for a_k with reasonably good performance [7]. For smaller values of BT_b, an ML sequence estimator or equalization must be used [4-6].

The first pseudo-symbol stream $a_{0,k} = a_k$ (we drop the first subscript since there are no other pulses) is related to the data symbols α_k by

$$a_n = \left(\sqrt{-1}\right)^{\sum_{m=0}^{n} \alpha_m}. \tag{6}$$

As a consequence, the pseudo symbols alternate between purely real (for even indices) and purely imaginary (for odd indices). For this reason, a slicer that follows that matched filter need only examine the real or imaginary parts of the matched filter output at alternating bit times.

Let $r(t) = z(t) + w(t)$ be the equivalent complex baseband received signal where $w(t)$ is a zero mean complex Gaussian random process whose real and imaginary parts have power spectral density $N_0/2$ Watt/Hz. The sampled matched filter outputs may be expressed as

$$x(kT_b) = p(k) + v(k) \tag{7}$$

where $p(k)$ denotes the contribution of the k-th data symbol as well as the adjacent $2(L+1)$ data symbols to the matched filter output. Thus $p(k)$ quantifies the intersymbol interference (ISI) at the matched filter output as illustrated in Figure 2. In this Figure, even-indexed points are clustered about the real axis and odd-indexed points are clustered about the imaginary axis. As BT_b increases, the severity of the ISI decreases and the clusters reduce to a single point. In the middle of each quadrant are both even- and odd-indexed points. These points are also due to ISI, which cross-correlates the real and imaginary components. By approximating the transmitted signal using only the first Laurent pulse, it is easy to show that $p(k)$ is approximated by

$$p(k) \approx \sum_{n=k-L}^{k+L} a_n R_h(-n) \tag{8}$$

where $R_h(n)$ is the deterministic autocorrelation function for the first Laurent pulse given by

$$R_h(n) = \int_0^{(L+1)T_b} h_0(t + nT_b) h_0(nT_b) dt. \tag{9}$$

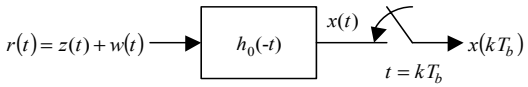

Figure 1. Structure of the "serial detector" based on a truncated Laurent representation.

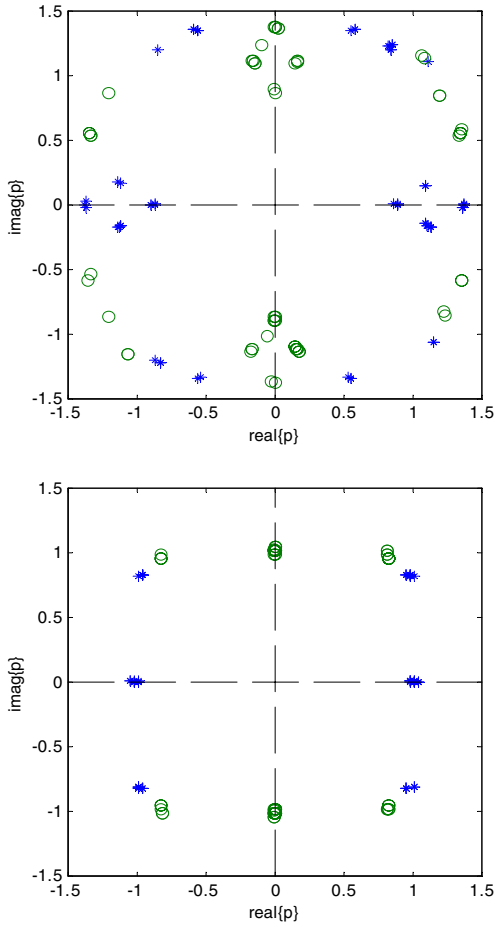

Figure 2. Data+ISI component of matched filter output for $BT_b = 1/5$, $L = 5$ (top) and $BT_b = 1/2$, $L = 2$ (bottom). The even indexed points are denoted by * and the odd indexed points by o.

The second term in (7) is due to noise and is given by

$$v(k) = \int_{kT_b}^{(L+1+k)T_b} w(t) h_0(t - kT_b)\,dt \,. \tag{10}$$

The sequence $v(k)$ is a sequence of correlated Gaussian random variables with autocorrelation function

$$R_v(n) = E\{v(k+n)v^*(k)\} = \sigma^2 R_h(n) \tag{11}$$

where $R_h(n)$ is given by (9) and where $\sigma^2 = N_0/2$.

III. Carrier Phase Estimation

A. ML Phase Estimation Observing the Received Signal

Let the received signal be given by

$$r(t) = z(t)e^{j\theta} + w(t) \tag{12}$$

where θ is the unknown carrier phase offset. We consider the case of data-aided carrier phase estimation where L_0 known data bits are available to aid the estimator. This scenario is common in burst mode applications where the known bits form a preamble or training sequence. Following the development in [8], the ML estimator for θ after observing $r(t)$ in the interval $0 \le t \le L_0 T_b$ is

$$\hat{\theta}_{\mathrm{ML}} = \arg\{\mathbf{a}^H \mathbf{x}\} \tag{13}$$

where $\mathbf{a} = [a_0 \quad a_1 \quad \cdots \quad a_{L_0-1}]^T$ is the column vector of pseudo symbols and $\mathbf{x} = [x(0) \quad x(1) \quad \cdots \quad x(L_0-1)]^T$ is the column vector of matched filter outputs. Mengali and D'Andrea [8] point out that this is only an approximate solution since the last L matched filter outputs result from integrations over a portion of the symbol since $h_0(t)$ spans $(L+1)T_b$ seconds. These "edge effects" diminish as the length of the training sequence increases or as BT_b increases. The edge effects cause the variance of the phase error estimate to increase. The reason the estimator performs worse is because the edge effects introduce a bias in the phase estimate. We derive an expression for this phase bias and demonstrate that proper compensation for the bias results in an estimator that achieves optimal performance as predicted by the Cramer-Rao bound.

To begin, let $\mathbf{x} = e^{j\theta}\mathbf{p} + \mathbf{v}$ where, $\mathbf{x}$ is the vector matched filter outputs, $\mathbf{p} = [p(0) \quad p(1) \quad \cdots \quad p(L_0-1)]^T$ is the vector representing the data+ISI contribution to the matched filter output and $\mathbf{v} = [v(0) \quad v(1) \quad \cdots \quad v(L_0-1)]^T$ is the vector of correlated noise samples at the matched filter output. The vector $\mathbf{v}$ consists of jointly Gaussian random variables with zero mean and autocovariance matrix $\mathbf{M}$ given by

$$\mathbf{M} = \sigma^2 \begin{bmatrix} R_h(0) & R_h(-1) & \cdots & R_h(-L_0+1) \\ R_h(1) & R_h(0) & \cdots & R_h(-L_0+2) \\ \vdots & \vdots & \ddots & \vdots \\ R_h(L_0-1) & R_h(L_0-2) & \cdots & R_h(0) \end{bmatrix} = \sigma^2 \mathbf{R}_h \,. \tag{14}$$

Using these definitions, the data term $\mathbf{a}^H\mathbf{x}$ may be expressed as

$$\mathbf{a}^H\mathbf{x} = \mathbf{a}^H\left(e^{j\theta}\mathbf{p} + \mathbf{v}\right) = e^{j\theta}\mathbf{a}^H\mathbf{p}\left(1 + e^{-j\theta}\frac{\mathbf{a}^H\mathbf{v}}{\mathbf{a}^H\mathbf{p}}\right) \tag{15}$$

so that

$$\arg\{\mathbf{a}^H\mathbf{x}\} = \theta + \arg\{\mathbf{a}^H\mathbf{p}\} + \arg\left\{1 + e^{-j\theta}\frac{\mathbf{a}^H\mathbf{v}}{\mathbf{a}^H\mathbf{p}}\right\}. \tag{16}$$

This shows that $\arg\{\mathbf{a}^H\mathbf{x}\}$ consists of the true phase θ, a bias term $\arg\{\mathbf{a}^H\mathbf{p}\}$, and a noise term. The bias term, $\theta_{\mathrm{bias}} = \arg\{\mathbf{a}^H\mathbf{p}\}$, diminishes as the approximation (8) improves. In fact, if (8) were exact, then $\mathbf{p} = \mathbf{R}_h\mathbf{a}$ and $\theta_{\mathrm{bias}} = \arg\{\mathbf{a}^H\mathbf{p}\} = \arg\{\mathbf{a}^H\mathbf{R}_h\mathbf{a}\} = 0$.

The noise term contains the complex-valued random variable $u = e^{-j\theta}\frac{\mathbf{a}^H\mathbf{v}}{\mathbf{a}^H\mathbf{p}}$ which is a zero-mean Gaussian random variable whose real and imaginary parts have variance $\frac{1}{2E_b/N_0}\frac{\mathbf{a}^H\mathbf{R}_h\mathbf{a}}{\left|\mathbf{a}^H\mathbf{p}\right|^2}$. The last term in (16) may be expressed as

$$\arg\left\{1 + e^{-j\theta}\frac{\mathbf{a}^H\mathbf{v}}{\mathbf{a}^H\mathbf{p}}\right\} = \arg\{1+u\} = \tan^{-1}\left(\frac{\mathrm{Im}\{u\}}{1+\mathrm{Re}\{u\}}\right) \approx \mathrm{Im}\{u\} \tag{17}$$

where the last approximation holds for L_0 sufficiently large so that the variance of $\mathrm{Im}\{u\}$ and $\mathrm{Re}\{u\}$ are small relative to 1. Taking the bias into account, the ML estimate is redefined to be

$$\hat{\theta}_{\mathrm{ML}} = \arg\{\mathbf{a}^H\mathbf{x}\} - \theta_{\mathrm{bias}} \,. \tag{18}$$

The mean and variance of the phase error $\hat{\theta}_{\mathrm{ML}} - \theta$ are

$$E\{\hat{\theta}_{\mathrm{ML}} - \theta\} \approx E\{\theta + \arg\{\mathbf{a}^H\mathbf{p}\} + \mathrm{Im}\{u\} - \arg\{\mathbf{a}^H\mathbf{p}\} - \theta\} = 0 \tag{19}$$

and

$$E\left\{\left|\hat{\theta}_{\mathrm{ML}} - \theta\right|^2\right\} \approx E\left\{\left|\theta + \arg\{\mathbf{a}^H\mathbf{p}\} + \mathrm{Im}\{u\} - \arg\{\mathbf{a}^H\mathbf{p}\} - \theta\right|^2\right\} = \frac{1}{2E_b/N_0}\frac{\mathbf{a}^H\mathbf{R}_h\mathbf{a}}{\left|\mathbf{a}^H\mathbf{p}\right|^2} \tag{20}$$

This shows that the estimator (18) is unbiased and has a variance inversely proportional to signal to noise ratio and L_0.

B. ML Phase Estimation Observing Matched Filter Outputs

The term $\mathbf{a}^H\mathbf{x}$ may be interpreted as an operation that de-rotates the matched filter output $\mathbf{x}$ by the phase of the data symbols. The idea is that any residual phase must be due to the

carrier phase θ. Since the data-dependent phase component of $\mathbf{x}$ is due to data and ISI, intuition suggests that a de-rotation by $\mathbf{p}$ rather than $\mathbf{x}$ would eliminate the need to subtract the bias from the phase estimate. This suggests the estimator

$$\hat{\theta}_{\mathrm{MF}} = \arg\left\{\mathbf{p}^H \mathbf{x}\right\} \tag{21}$$

where the subscript "MF" means "matched filter." Substituting $\mathbf{x} = e^{j\theta}\mathbf{p} + \mathbf{v}$ produces

$$\mathbf{p}^H \mathbf{x} = \mathbf{p}^H \left(e^{j\theta}\mathbf{p} + \mathbf{v}\right) = e^{j\theta}\mathbf{p}^H \mathbf{p}\left(1 + e^{-j\theta}\,\frac{\mathbf{p}^H \mathbf{v}}{\mathbf{p}^H \mathbf{p}}\right) \tag{22}$$

so that

$$\arg\left\{\mathbf{p}^H \mathbf{x}\right\} = \theta + \arg\left\{\mathbf{p}^H \mathbf{p}\right\} + \arg\left\{1 + e^{-j\theta}\,\frac{\mathbf{p}^H \mathbf{v}}{\mathbf{p}^H \mathbf{p}}\right\}. \tag{23}$$

Since $\mathbf{p}^H \mathbf{p}$ is real, the estimate $\hat{\theta}_{\mathrm{MF}}$ is unbiased. The variance of the estimator is

$$\mathrm{E}\left\{\left|\theta - \hat{\theta}_{\mathrm{MF}}\right|^2\right\} = \frac{1}{2E_b / N_0}\,\frac{\mathbf{p}^H \mathbf{R}_h \mathbf{p}}{\left|\mathbf{p}^H \mathbf{p}\right|^2}. \tag{24}$$

In the next section, we demonstrate the variance of this estimator is larger than that of the ML estimator (18). The reason for the loss in performance is that the MF estimator (21) does not account for the correlation of the noise samples. The correlation can be incorporated into the phase estimate by formulating an ML estimator based on an observation of L_0 matched filter outputs.

The conditional probability $f(\mathbf{x} \mid \mathbf{a}, \theta)$ is

$$f(\mathbf{x} \mid \theta, \mathbf{a}) = \frac{1}{(2\pi)^{L_0/2}\left|\sigma^2 \mathbf{R}_h\right|^{1/2}} \exp\left\{-\frac{1}{2\sigma^2}\left(\mathbf{x} - e^{j\theta}\mathbf{p}\right)^H \mathbf{R}_h^{-1}\left(\mathbf{x} - e^{j\theta}\mathbf{p}\right)\right\}. \tag{25}$$

Computing the derivative of $\ln\left(f(\mathbf{x} \mid \mathbf{a}, \theta)\right)$ with respect to θ, setting it to zero, and solving for θ produces the estimator

$$\hat{\theta}_{\mathrm{ML\text{-}2}} = \arg\left\{\mathbf{p}^H \mathbf{R}_h^{-1} \mathbf{x}\right\}. \tag{26}$$

Substituting $\mathbf{x} = e^{j\theta}\mathbf{p} + \mathbf{v}$ produces

$$\mathbf{p}^H \mathbf{R}_h^{-1} \mathbf{x} = \mathbf{p}^H \mathbf{R}_h^{-1}\left(e^{j\theta}\mathbf{p} + \mathbf{v}\right) = e^{j\theta}\mathbf{p}^H \mathbf{R}_h^{-1}\mathbf{p}\left(1 + e^{-j\theta}\,\frac{\mathbf{p}^H \mathbf{R}_h^{-1}\mathbf{v}}{\mathbf{p}^H \mathbf{R}_h^{-1}\mathbf{p}}\right) \tag{27}$$

so that

$$\arg\left\{\mathbf{p}^H \mathbf{R}_h^{-1} \mathbf{x}\right\} = \theta + \arg\left\{\mathbf{p}^H \mathbf{R}_h^{-1}\mathbf{p}\right\} + \arg\left\{1 + e^{-j\theta}\,\frac{\mathbf{p}^H \mathbf{R}_h^{-1}\mathbf{v}}{\mathbf{p}^H \mathbf{R}_h^{-1}\mathbf{p}}\right\}. \tag{28}$$

Since $\mathbf{p}^H \mathbf{R}_h^{-1}\mathbf{p}$ is real, the estimate $\hat{\theta}_{\mathrm{ML-2}}$ is unbiased. The variance of the estimator is

$$\mathrm{E}\left\{\left|\theta - \hat{\theta}_{\mathrm{ML\text{-}2}}\right|^2\right\} = \frac{1}{2E_b / N_0}\,\frac{1}{\mathbf{p}^H \mathbf{R}_h^{-1}\mathbf{p}}. \tag{29}$$

IV. Numerical Results

The behavior of the ML estimate bias as a function of BT_b and the training sequence length L_0 is illustrated in Figure 3. This plot demonstrates that the bias increases with decreasing BT_b and/or decreasing L_0. Both of these trends are due to the "edge effects" discussed previously and described in [8]. As BT_b decreases, length of the first Laurent pulse increases. As a consequence, the number of points in the vector $\mathbf{p}$ resulting from "partial integrations" increases. As L_0 decreases, the overall influence of the partial integrations increases.

The performance of the ML estimators (13) and (18) is illustrated in Figure 4 for BT_b = 1/5 and L_0 = 64. The performance predicted by (20) is plotted (the solid line) along with the Cramer-Rao bound (dashed line). The Cramer-Rao bound is not visible since it coincides with the plot of (20). Simulation results are included where we observe that the performance of the estimator (13), which neglects the bias, departs from the Cramer-Rao bound for $E_b/N_0 > 5$ dB. For this combination of BT_b and L_0, $E_b/N_0 > 5$ dB is the region where the contribution to phase error due to the uncompensated bias swamps the contribution due to thermal noise. Simulation results for the estimator (18), which includes the bias, show that the bias compensation allows the estimator to achieve the Cramer-Rao bound.

A performance comparison of the three estimators $\hat{\theta}_{\mathrm{ML}}$, $\hat{\theta}_{\mathrm{MF}}$, and $\hat{\theta}_{\mathrm{ML\text{-}2}}$ defined by Equations (18), (21), and (26), respectively, is illustrated in Figure 5. The phase error variances for the three given in Equations (20), (24), and (29) are plotted along with simulation results. The simulation results track the predicted performance. Note that the heuristic estimator $\hat{\theta}_{\mathrm{MF}}$ has a higher phase error variance than the other two. The two ML estimators have essentially the same performance. This is to be expected since they are both based on the maximum likelihood principle.

V. Conclusions

Data-aided carrier phase estimation for GMSK using the serial or MSK-type detector has been examined. Previously published ML solutions were approximate since partial integrations produced edge effects that reduced the performance of the estimator. The contribution of edge effects was shown to produce a bias in the ML estimator. Once the bias was removed, the performance of the new ML estimator achieved the Cramer-Rao bound [12].

Two alternate solutions were also introduced: one heuristic (called the MF estimator) and the other based on the maximum likelihood principle (called the ML-2 estimator) [12]. The performance of the ML-2 estimator matches that of the modified ML estimator. In fact, the performance of the two is

identical when the approximation (8) is replaced by equality. In this case $\mathbf{p} = \mathbf{R}_h\mathbf{a}$ and the phase error variances are

$$E\left\{\left|\theta-\hat{\theta}_{\mathrm{ML}}\right|^2\right\} = E\left\{\left|\theta-\hat{\theta}_{\mathrm{ML\text{-}2}}\right|^2\right\} = \frac{1}{2E_b/N_0}\frac{1}{\mathbf{a}^H\mathbf{R}_h\mathbf{a}}.$$

The performance of the MF estimator is inferior to the other two.

The complexity of the ML-2 estimator is significantly greater than that of the ML estimator since the ML-2 estimator requires a full-width multiplier to form the dot product. The ML estimator, on the other hand, only requires adds since the pseudo symbols are in the set $\{-1,+1,-j,+j\}$.

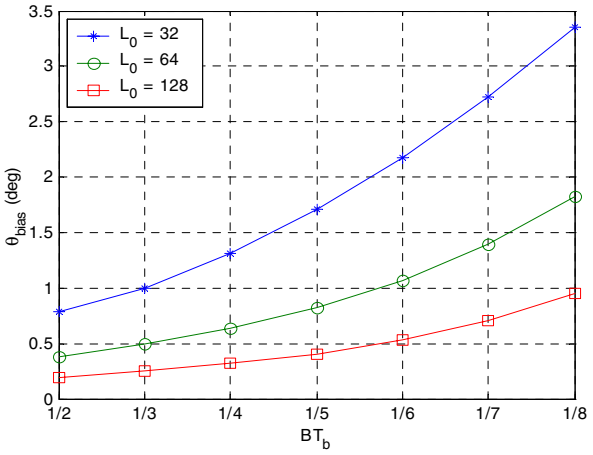

Figure 3. Phase estimator bias as a function of BT_b and training seqeunce length L_0. 10,000 random sequences were generated and the phase bias was computed for each one using BT_b=1/5 and L = 5. The sequence with the largest phase bias was used to generate these plots.

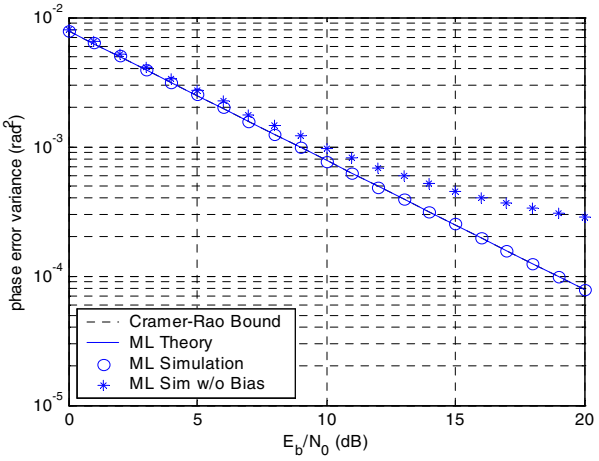

Figure 4. Performance of the ML estimator for BT_b = 1/5, L= 5, and L_0 = 64. The data sequence used was the same one used in Figure 3.

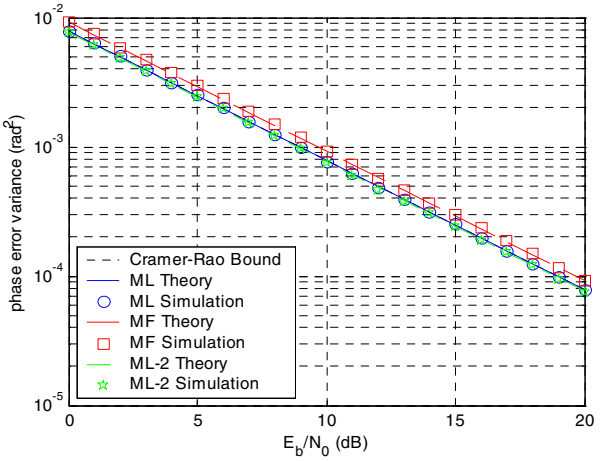

Figure 5. Performance comparison of the ML, MF, and ML-2 estimators for BT_b = 1/5, L= 5, and L_0 = 64.

VI. REFERENCES

[1] K. Tsai and G. Lui, "Binary GMSK: Characteristics and Performance," in *Proceedings of the International Telemetering Conference*, Las Vegas, NV, October 1999.

[2] P. Laurent, "Exact and Approximate Construction of Digital Phase Modulations by Superposition of Amplitude Modulated Pulses (AMP)," *IEEE Transactions on Communications*, vol. 34, no. 2, February 1986, pp 150-160.

[3] J. Proakis, *Digital Communications*, McGraw-Hill, New York, 2001.

[4] G. Kaleh, "Simple Coherent Receiver for Partial Response Continuous Phase Modulation," *IEEE Journal on Selected Areas in Communications*, vol. 7, no. 9, December 1989, pp. 1427-1436.

[5] G. Lui and K. Tsai, "Viterbi and Serial Demodulators for Pre-Coded Binary GMSK," in *Proceedings of the International Telemetering Conference*, Las Vegas, NV, October 1999.

[6] G. Lui and K. Tsai, "Data-Aided Symbol Time and Carrier Phase Tracking For Pre-Coded CPM Signals," in *Proceedings of the International Telemetering Conference*, Las Vegas, NV, October 1999.

[7] G. Lui, "Threshold Detection Performance of GMSK Signal With BT=0.5," in *Proceedings of IEEE MILCOM*, Boston, MA, October 1998.

[8] U. Mengali and A. D'Andrea, *Synchronization Techniques for Digital Receivers*, Plenum, New York, 1997.

[9] M. Simon, "MAP-Motivated Carrier Synchronization of GMSK Based on the Laurent AMP Representation," in *Proceedings of IEEE GLOBECOM*, 1998.

[10] J. Huber and W. Liu, "Data-Aided Synchronization of Coherent CPM-Receivers," *IEEE Transactions on Communications*, vol. 40, no. 1, January 1992.

[11] R. Bow, "Hardware Performance for Binary GMSK With BT=1/5," in *Proceedings of the International Telemetering Conference*, Las Vegas, NV, October 1999.

[12] Patent application in process, initial disclosure date 2 July 2002.